

Unitarity Corrections to the Drell-Yan Process in the Target Rest Frame

M.A. Betemps*, **M.B. Gay Ducati[†]** and **M.V.T. Machado[‡]**

*Instituto de Física, Universidade Federal do Rio Grande do Sul.
Postal Box 15051, CEP 91501-970. Porto Alegre, RS, BRAZIL.*

ABSTRACT: The unitarity corrections effects encoded in the Glauber-Mueller approach are taken into account to calculate the differential cross sections in the Drell-Yan process in the rest frame. A detailed study of the Drell-Yan process in terms of the γ^*q transverse separation and the color dipole size, as well as the effective dipole cross section is performed and compared with the available small x data. Estimates for the Drell-Yan cross section at RHIC energies are presented and discussed.

KEYWORDS: Drell-Yan process; Perturbative calculations; Unitarity corrections .

*E-mail:mandrebe@if.ufrgs.br

[†]E-mail:gay@if.ufrgs.br

[‡]E-mail:magnus@if.ufrgs.br

1. Introduction

Both the massive lepton pairs production in hadronic collisions (Drell-Yan) and deep inelastic scattering (DIS) at high energy are the most outstanding processes probing the hadron structure. On the deep inelastic side, a large amount of work has been done to describe the copious data at medium and very small Bjorken scaling variable x based on perturbative QCD [1]. In the high energy domain it has been found that important unitarity corrections should be taken into account regarding the standard pQCD approach [2]. These phenomena is currently denominated perturbative shadowing or saturation effects [3, 4, 5, 6]. Concerning the Drell-Yan sector, the pQCD tools have produced a reasonable theoretical understanding of the main observables, despite the small data set available at the present [7]. The forthcoming accelerator experiments (RHIC and LHC) will scan the high energy limit of the hadronic reactions and open a new kinematic window, i.e. smaller x values. In particular, the quark-gluon plasma (QGP), a new state of the hadronic matter predicted by QCD, is expected to be found there [8]. The theoretical description of the QGP production is directly associated to a complete knowledge about saturation effects in the transition region to the high parton densities. In particular, since the production scheme for J/Ψ is similar to the Drell-Yan one and the latter does not contain final state effects, DY can be considered a baseline process to study J/Ψ suppression as a signature of QGP formation [9].

In the fast proton system, the QCD factorization theorem describes the hadronic processes through the convolution of the parton distribution functions (pdf's) with the partonic subprocesses. The latter are completely calculated in pQCD up to higher orders, whereas only the evolution in the factorization scale of the pdf's is determined. Namely, the parton distributions are solutions of the DGLAP evolution equations, whose formalism has been successfull to describe both DIS and DY data [1, 7]. Recently, an alternative way to study electron-proton and hadronic reactions is claimed by the color dipole picture considering the rest frame description based on k_T -factorization [3, 10, 11]. Thus the basic blocks are the dipole light-cone wavefunction and the dipole-target cross section. Such an approach has produced an unified way to study the mentioned processes, however its complete connection with the standard DGLAP formalism is not provided yet and deserves further studies.

In the infinite momentum frame, the DY process corresponds to the annihilation of projectiles quark (antiquark) with antiquark (quark) of the target into a virtual photon (vector boson), which afterwards decays into a lepton pair [12]. In the leading order (LO) calculation, Drell-Yan has a simple electromagnetic character and it can be promptly given by QED theory. However, from QCD the perturbative results at higher orders just destructs this simple picture. At present, pQCD calculations have been developed up to α_s^2 order of the strong coupling constant [13]. For practical considerations, in general the involved next orders contributions are taken into ac-

count by a phenomenological parameter, namely the so called K factor dependent on the DY kinematic variables.

In the rest frame, DY process looks like a bremsstrahlung of a virtual photon decaying into a lepton pair, rather than a parton annihilation [11]. The bremsstrahlung of the virtual photon can occur after or before the interaction with the gluonic field of the target. The great advantage of this formalism is that the corresponding cross section can be considered in terms of the same dipole cross section extracted of small- x DIS at the color dipole picture [14]. At high energy, the unitarity corrections should be included in the dipole cross section. Such effects have been considered for example in the phenomenological model of G.Biernat-Wusthoff (GBW) [15], which describes DIS and ep diffractive process with good agreement. However, the main disadvantage in GBW is that a dynamical explanation of the saturation phenomena is lacking. On the other hand, the Glauber-Mueller approach provides a well established theoretical development concerning parton saturation [4], constraining the pQCD description of the dipole cross section. Here, we make use of this formalism to perform a description of DY process at the rest frame.

The goal of this work is to perform a study of DY at high energies considering the color dipole picture, in a similar way of the recent works [16]. We use the dipole cross section calculated in perturbative QCD, through the Glauber-Mueller formula [4], which encodes the unitarity effects (saturation) in the parton densities. This approach takes into account the multiple Pomeron scattering hypothesis in an eikonal way keeping the unitarity of the considered process. A comparison between the phenomenological GBW dipole cross section and the theoretical Glauber-Mueller one is presented, verifying that the two approaches have different behaviors at higher energies. This is due to the dynamical dependence on the gluon distribution in the Glauber-Mueller approach, whose Born term recovers the DGLAP kernel at double log approximation (DLA). The nonperturbative region, i.e. large dipole sizes contributions, is addressed considering the freezing of the gluon distribution under the initial perturbative evolution scale Q_0^2 . Then, we present DY calculations in the rest frame of the target at leading order in a pp collision and perform a comparison with the low x DY differential cross section from the E772 Collaboration [17]. We also produce estimates for the cross section at RHIC energies.

The outline of this paper is the following. In the next section we present a brief review of the DY process in the dipole color picture, discussing the range of validity for this approach and showing the role played by the γ^*q wavefunction. In Sec. (3) we present the high parton density effects calculated from the Glauber-Mueller approach, and confronting it with the phenomenological GBW model. We estimate the contribution of the saturation effects for the dipole cross section in high energies (those ones reached at LHC and RHIC). In Sec. (4), a parameter-free prediction to the differential DY cross section for the available data at small- x and estimates to RHIC are performed. Finally, in the last section one discusses the results and

presents our conclusions.

2. Drell-Yan in the Color Dipole Picture

Before the description of the Drell-Yan process in the rest frame, we would like to review the main kinematical variables and the standard calculations in the laboratory system. This is important to clarify the connection between them and to explicit the asymmetry projectile-target in the rest frame picture.

In the laboratory system, the lepton pairs are produced in the Drell-Yan reaction where partons from the projectile (fast proton) interact with the proton target [12]. Looking at the parton level, a quark-antiquark pair annihilates into a virtual photon at leading order ($q\bar{q} \rightarrow \gamma^* \rightarrow l^+l^-$). The symmetry between target and projectile is very clear, namely we cannot distinguish a quark coming from the proton target or from the incoming beam. The momentum fraction carried by the quark from the projectile is labeled x_1 and from the target one is named x_2 . The partonic subprocess above is well known from QED, and the hadroproduction cross section is obtained folding the partonic cross section with the quark (antiquark) densities evaluated at the invariant M^2 , the squared lepton pair mass, chosen here as the factorization scale μ_{fac}^2 . Their evolution in M^2 is given by the standard DGLAP evolution equations. Therefore, the DY differential cross section at leading order is given by,

$$\frac{d^2\sigma^{DY}}{dM^2 dx_F} = \frac{4\pi\alpha_{\text{em}}^2}{9M^2 s} \frac{1}{(x_1 + x_2)} \sum_f e_f^2 \left[q_f(x_1, M^2) \bar{q}_f(x_2, M^2) + \bar{q}_f(x_1, M^2) q_f(x_2, M^2) \right],$$

where $q[\bar{q}]_f(x, M^2)$ are the corresponding quark (antiquark) densities with flavour f and squared charge e_f^2 . The center of mass energy squared is s and the usual notation is

$$x_F = x_1 - x_2, \tag{2.1}$$

$$\tau = x_1 x_2 = M^2/s. \tag{2.2}$$

The momentum fractions are rewritten as

$$x_1 = \frac{1}{2}(\sqrt{x_F^2 + 4\tau} + x_F), \tag{2.3}$$

$$x_2 = \frac{1}{2}(\sqrt{x_F^2 + 4\tau} - x_F), \tag{2.4}$$

where x_F is the longitudinal momentum fraction, labeled Feynman x . Indeed, x_F , M and s are the true kinematic variables experimentally measured, whereas the partonic variables, x_1 and x_2 , are reconstructed from them.

When we consider the target at rest, the DY process looks like a bremsstrahlung: the quark from the projectile radiates a photon, which carries a fraction α of the

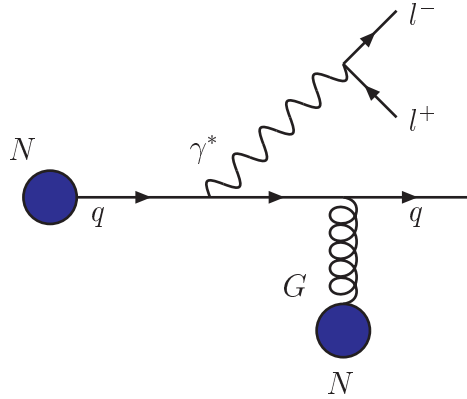


Figure 1: The Drell-Yan process in the rest frame, depicting one of the possible interactions $\gamma^* q$ -target (see text).

light-cone momentum of the initial quark, thus after decays into the lepton pair [see Fig. (1)]. The interaction with the target can occur before or after the photon emission. Thus, although diagrammatically no dipole is present, the interference among graphs results in a product of two quark amplitudes in the DY cross section, testing the external gluonic field at two different transverse positions [11]. Therefore, a remarkable feature emerging is that the $\gamma^* q - N$ interaction can be described by the same dipole cross section as in DIS [14].

In the impact parameter representation, the photoabsorption cross section in deep inelastic is described by the convolution of the wavefunctions, Ψ_{γ^*} , from the virtual photon and the interaction dipole cross section, $\sigma_{q\bar{q}}$. The wavefunctions are considered taking into account the first photon Fock state configuration, namely a $q\bar{q}$ pair. The dipole cross section is modeled phenomenologically based on a matching between the hard and soft pieces, constrained by the DIS available data. The transverse separation of the $q\bar{q}$ pair is r_\perp , and each quark (or antiquark) of the dipole carries a momentum fraction α (or $1 - \alpha$), from the incoming photon. The small dipole size configurations can be described through pQCD, whereas the large size ones belong to the nonperturbative domain. Hence, one can write the photoabsorption cross section as a function of the scaling variable x and photon virtuality Q^2 in the quantum mechanics form [10],

$$\sigma_{T,L}(\gamma^* p \rightarrow q\bar{q}) = \int d^2 r_\perp \int_0^1 d\alpha |\Psi_{q\bar{q}}^{T,L}(\alpha, r_\perp)|^2 \sigma_{q\bar{q}}(x, r_\perp) , \quad (2.5)$$

where T, L indicate the transverse and longitudinal contributions to the total cross section. In a similar way, the cross section for radiation of a virtual photon from a quark after scattering on a proton, has the following factorized form in impact

parameter representation [11],

$$\frac{d\sigma_{T,L}(qp \rightarrow \gamma^* X)}{d\ln\alpha} = \int d^2r_\perp |\Psi_{\gamma^*q}^{T,L}(\alpha, r_\perp)|^2 \sigma_{q\bar{q}}(x_2, \alpha r_\perp), \quad (2.6)$$

where we have the same dipole cross section as in DIS. Here r_\perp is the photon-quark transverse separation, αr_\perp is the $q\bar{q}$ separation and α is the fraction of the light-cone momentum of the initial quark taken away by the photon. Note the difference with the DIS case, where the dipole separation is just r_\perp . Here, $\sigma_{q\bar{q}}$ is the cross section for scattering a $q\bar{q}$ pair off a proton which depends on the $q\bar{q}$ transverse separation and which should take into account the saturation effects at high energy.

The physical interpretation of (2.6) is similar to DIS in the light-cone approach (LC). The projectile quark is expanded in its Fock space in the form [11],

$$|q\rangle = Z_2|q\rangle + \Psi_{\gamma^*q}^{T,L}|q\gamma^*\rangle + \dots \quad (2.7)$$

where here one has the expansion in terms of the eigenstates from the incident quark. Instead, in deep inelastic the expansion is constructed from the eigenstates of the incident photon [10].

The LC wavefunctions can be calculated in perturbation theory and are well known [10, 11]. They depend on the transverse separations and momentum fraction α . They play an important role in the dilepton mass M dependence. We take the same notation for the LC wavefunctions from [16],

$$|\Psi_{\gamma^*q}^T(\alpha, r_\perp)|^2 = \frac{\alpha_{\text{em}}}{\pi^2} \left(m_f^2 \alpha^4 K_0^2(\eta r_\perp) + [1 + (1 - \alpha)^2] \eta^2 K_1^2(\eta r_\perp) \right), \quad (2.8)$$

$$|\Psi_{\gamma^*q}^L(\alpha, r_\perp)|^2 = \frac{2\alpha_{\text{em}}}{\pi^2} M^2 (1 - \alpha)^2 K_0^2(\eta r_\perp). \quad (2.9)$$

The functions K_0 and K_1 are the modified Bessel functions and the auxiliary variable η , depending on the quark mass m_f is given by

$$\eta^2 = (1 - \alpha)M^2 + \alpha^2 m_f^2. \quad (2.10)$$

The hadronic differential cross section for the Drell-Yan process is expressed in the factorized form [11],

$$\frac{d\sigma^{DY}}{dM^2 dx_F} = \frac{\alpha_{\text{em}}}{6\pi M^2} \frac{1}{(x_1 + x_2)} \int_{x_1}^1 \frac{d\alpha}{\alpha} F_2^p\left(\frac{x_1}{\alpha}\right) \frac{d\sigma(qp \rightarrow q\gamma^* p)}{d\ln\alpha} \quad (2.11)$$

The factor $\alpha_{\text{em}}/(6\pi M^2)$ is due to the photon decay into the lepton pair, coming from electrodynamics, the differential cross section $d\sigma(qp \rightarrow q\gamma^* p)/d\ln\alpha$ is taken from equation (2.6) and our input to $\sigma_{q\bar{q}}$ in this work [4] is given by the standard gluon distribution in the target corrected by saturation effects at high energy limit. In Eq. (2.11), the structure of the projectile is described by the $F_2^p(x, Q^2)$ structure function.

Here, some comments are in order. In the rest frame, the process is asymmetric concerning projectile and target, in contrast with the symmetric picture in the Breit frame. The dipole color picture is valid for small x_2 and it takes into account only the gluonic (sea quarks) sector from the target, disregarding its valence content. However, both valence and sea quarks in the projectile are parametrized in the proton structure function in Eq. (2.11) (for a complete discussion see Refs. [16]).

Although at present there are little range of experimental measurements in the kinematical limit of validity of the color dipole approach, it should provide reasonable results when one considers smaller x_2 than the currently available. The high energy accelerators LHC and RHIC will open a wider kinematical window towards smaller x_2 values allowing to test rest frame calculations properly.

To conclude this section, we analyse the behavior of the wavefunctions in the relevant kinematic variables. As we will see, they play the role of a weight to the dipole cross section concerning the transverse separations. In Eqs. (2.5-2.6), large r_\perp configurations are suppressed in the integrated cross section, controlling the non-perturbative contributions (large transverse distances domain) to the observables. In the deep inelastic case, the LC wavefunctions dependence on the radius r_\perp at fixed photon virtuality Q^2 is discussed in Refs. [18]. For the Drell-Yan case, the weight function is given by:

$$W_{\gamma^*q}^{T,L}(r_\perp, M^2) = r_\perp \int \frac{d\alpha}{\alpha} F_2^p(x_1/\alpha, M^2) |\Psi_{\gamma^*q}^{T,L}(\alpha, r_\perp)|^2. \quad (2.12)$$

In Fig. (2) one shows separately the longitudinal and transverse results for $W^{T,L}(r_\perp, M^2)$ as a function of the photon-quark transverse separation r_\perp at fixed lepton pair mass M . The chosen momentum fraction was $x_1 \approx x_F = 0.525$, since it is a typical experimental value measured (see Sec. 4). Considering this x_1 value, the proton structure function is insensitive to the lepton pair mass range because it is in the scaling region. Regarding the quark mass, here one takes an effective light quark mass $m_f = 0.2$ GeV in the wavefunctions.

For the transverse contribution, the upper plot in Fig. (2), one verifies that the weight function selects small to intermediate photon-quark sizes. This means it is selecting small dipole sizes (αr_\perp) in a similar way to deep inelastic, since $0 \leq \alpha \leq 1$. A steep increasing as $r_\perp \rightarrow 0$ comes from the behavior of the function $K_1(\eta r_\perp) \sim 1/(\eta r_\perp)$ at this limit. Concerning the dependence on M , as the invariant mass increases the contribution looks smaller.

Regarding the longitudinal piece, the lower plot in Fig. (2), the weight function selects smaller dipole sizes (and γ^*q transverse sizes) in comparison with the transverse one. Moreover, the function is narrower as M increases, meaning that larger invariant mass scans smaller r_\perp . A well known fact is that the longitudinal contribution is higher twist, i.e. it is suppressed by a power of $1/M^2$ when compared with the transverse one [10]. This feature actually remains in the Drell-Yan case. Moreover,

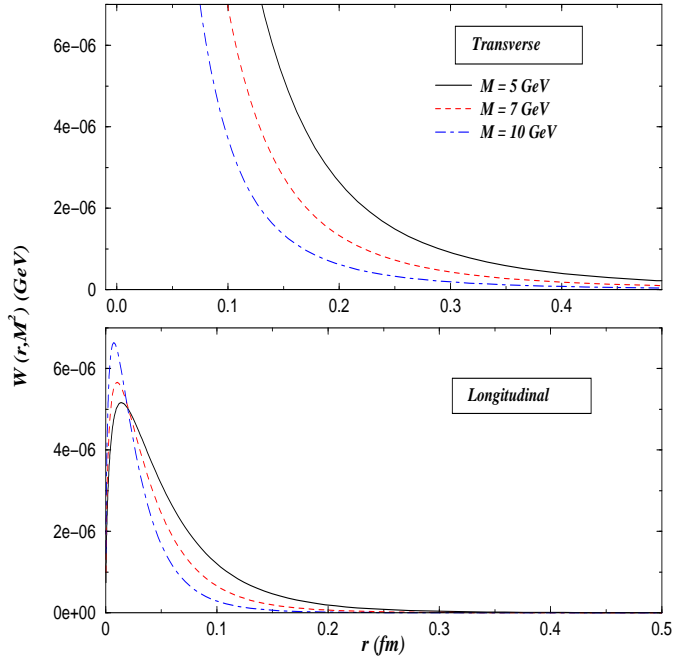


Figure 2: The longitudinal and transverse contributions for $W(r_\perp, M^2)$ as a function of the γ^*q transverse size r_\perp at fixed lepton pair mass M , for $x_1 \approx x_F = 0.525$.

the peaks appearing in the plot are due to the balancing between the asymptotic behavior at $r_\perp \rightarrow 0$ of the function $K_0(\eta r_\perp) \sim -\log(\eta r_\perp)$ and the linear r_\perp factor in Eq. (2.12).

Having addressed the main features from the color dipole framework, namely kinematic definitions and the description of Drell-Yan process in the rest frame, in the next section one introduces our model for the dipole cross section satisfying unitarity requirements.

3. The Glauber-Mueller Approach

The cross section for a color dipole-nucleon scattering is a well known quantity, which was first proposed in the BFKL framework [19]. The dipole interacts with the target through a perturbative Pomeron, described in terms of the ladder diagrams. From the k_T -factorization framework [20], the scattering process can be written as the convolution of the projectile impact factor and the unintegrated gluon structure function from the target, whose dynamics is determined by the evolution kernel. The possible orderings on the transverse momentum k_T in these graphs produce the DGLAP or the BFKL dynamical evolutions. In particular, considering small r_\perp configurations from the dipole and the k_T -factorization one obtains,

$$\sigma_{q\bar{q}}(x, r_\perp) = \frac{\pi^2 \alpha_s}{3} r_\perp^2 x G_N^{DGLAP}(x, \frac{4}{r_\perp^2}) \quad (3.1)$$

where $xG_N^{DGLAP}(x, \tilde{Q}^2)$ is the standard DGLAP gluon distribution at momentum fraction x and virtuality scale $\tilde{Q}^2 = 4/r_\perp^2$. An extensive phenomenology has been made using the result above for inclusive structure function and vector meson production [18]. In particular, we call attention for the specific value of the scale r_0^2 appearing in the virtuality scale $\tilde{Q}^2 = r_0^2/r_\perp^2$. We use the $r_0^2 = 4$ throughout this paper, however other values are equivalent at leading logarithmic level [18].

A well defined feature from the data on F_2 and on the gluon distribution at high energies, i.e. smaller x , is that they present a steep increasing as x decreases. Indeed, experimentally $F_2 \sim xG \sim x^{-\lambda}$, where the exponent ranges from 0.08 (Regge phenomenology) up to 0.5 (LO BFKL calculations). Such a behavior extrapolated to asymptotic energies violates unitarity requirements in a theoretical point of view and a control should be considered. The scale where these effects start to be important is associated to a region between hard and soft dynamics [21] (pQCD versus Regge) or belonging to the high density QCD domain [4]. Here, we are interested in the last case (for a recent review, see [22]). In QCD, the taming of the gluon distribution at high energies is taken into account through multiple Pomeron scattering encoded in the eikonal-like frameworks [23]. Such a procedure provides the unitarization of the Born Pomeron cross section leading to a softer growth with energy. Indeed, the asymptotic calculations have produced an unified $\ln(1/x)$ pattern for the cross section and gluon function instead of a truly saturated one [24].

In this work we use Eq.(3.1), where the standard DGLAP gluon distribution is substituted by the corrected one, considering the unitarity corrections given by the Glauber-Mueller approach, $xG^{GM}(x, \frac{4}{r_\perp^2})$ (see Ref. [4]). It has also an implicit dependence on the target radius R , whose value is extracted from the experimental data. For more details concerning these issues in the color dipole picture, we address Ref. [25].

Now, one discusses in a detailed way the main characteristics emerging from the Glauber-Mueller dipole cross section. To do this, in Fig. (3) one shows the Glauber-Mueller dipole cross section as a function of dipole transverse size $r = \alpha r_\perp$ at fixed momentum fraction x_2 . For sake of a better illustration on the partonic saturation effects, we choose a very small value for $x = 10^{-6}$. Hereafter, we are using the GRV gluon distribution at leading order [26]. The solid line corresponds to the standard DGLAP calculation (without saturation), Eq. (3.1), whereas the remaining ones result from unitarity corrections for two different target size. The general shape in terms of the dipole size comes from the balancing between the color transparency $\sigma \sim r_\perp^2$ behavior and the gluon distribution shape. These features are depicted in the plots in Fig. (4), where one verifies a visible scaling of $xG(x, \tilde{Q}^2)$ versus \tilde{Q}^2 (left plot) and its dependence on $r = \alpha r_\perp$ (right plot).

The difference in the strength of the unitarity corrections associated with the target size is a well known fact. From the data analysis, its value ranges from $R^2 = 5 - 10 \text{ GeV}^{-2}$, where smaller radius produces strongest corrections [see Fig.

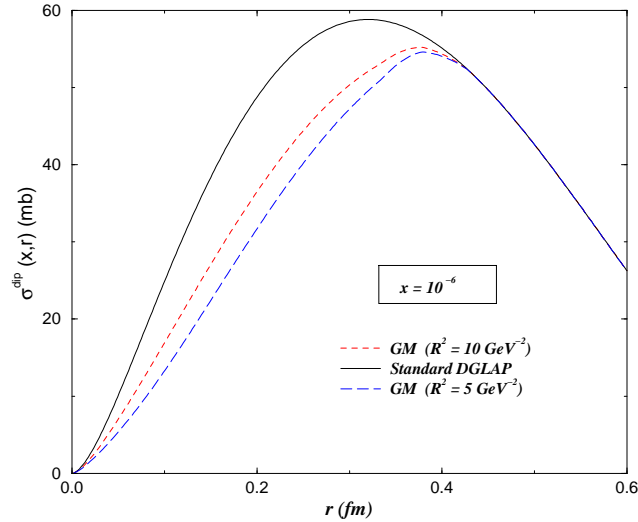


Figure 3: The color dipole cross section as a function of the dipole size $r = \alpha r_\perp$ at fixed $x_2 = 10^{-6}$. The solid line corresponds to the result without unitarity corrections. The dotted line is the GM prediction using $R^2 = 10 \text{ GeV}^{-2}$, whereas the dashed one is for $R^2 = 5 \text{ GeV}^{-2}$.

(3)]. For our calculations we choose the low value $R^2 = 5 \text{ GeV}^{-2}$, corroborated by studies in the inclusive structure function and its derivative [27].

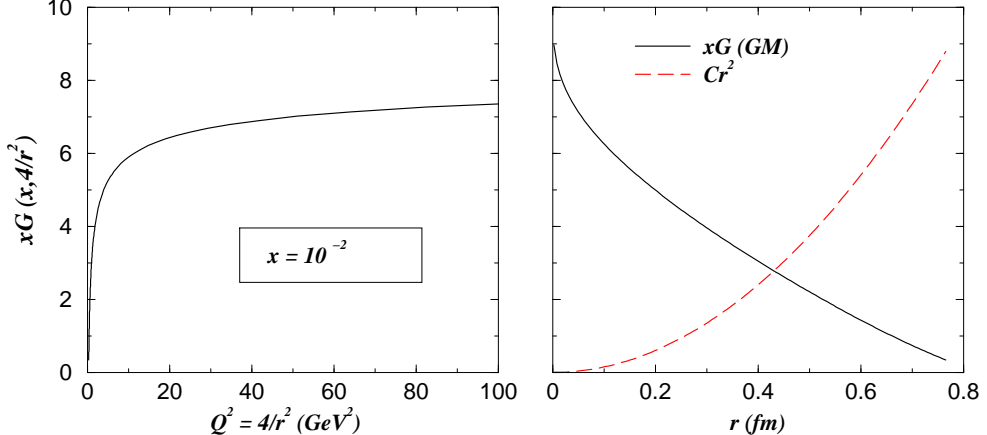


Figure 4: The plot on the left shows the GM gluon distribution (GRV parametrization input) as a function of the scale $\tilde{Q}^2 = 4/r^2$ at fixed $x = 10^{-2}$. On the right, GM gluon distribution versus r and the color transparency behavior $\sigma_{dip} \sim C r^2$ (for illustration one uses a free normalization $C = 15$).

For sake of comparison, we will consider the phenomenological model of Ref. [15] (GBW), which has produced a good description of HERA data in both inclusive and diffractive processes. It is constructed interpolating the color transparency behavior $\sigma_{dip} \sim r_\perp^2$ at small dipole sizes and a flat (saturated) behavior at large dipole sizes

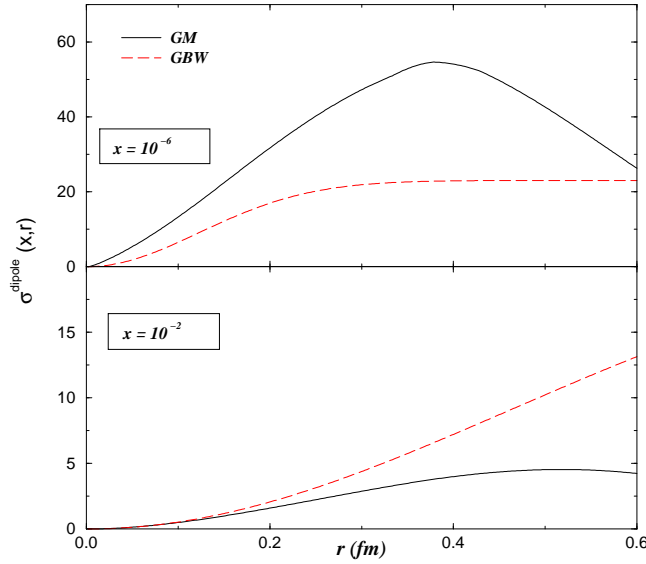


Figure 5: The GM dipole cross section as a function of the dipole size $r = \alpha r_\perp$ at two typical x_2 values. The GBW result is also shown for sake of comparison.

$\sigma_{dip} \sim \sigma_0$ (confinement). The expression has the eikonal-like form,

$$\sigma_{q\bar{q}}(x, r) = \sigma_0 \left[1 - \exp \left(\frac{r^2 Q_0^2}{4(x/x_0)^\lambda} \right) \right], \quad (3.2)$$

where $Q_0^2 = 1$ GeV 2 and the three fitted parameters are $\sigma_0 = 23.03$ mb, $x_0 = 3.04 \cdot 10^{-4}$ and $\lambda = 0.288$ and $R_0(x) = (x/x_0)^{\lambda/2}$ is the saturation radius. The resulting GBW total cross section lies below the typical hadronic cross section, namely $\sigma_{\pi N}^{GBW} \leq \sigma_{\pi N}$. Despite describing the data in good agreement, GBW does not present a dynamical hypothesis for the saturation phenomena and does not match DGLAP evolution. In GBW, saturation is characterized by the x -dependent saturation radius $Q_s^2(x) = 1/R_0^2(x)$ instead of the most involved scale coming from Glauber-Mueller, $\kappa_G(x, Q_s^2) = 1$, which can be easily extended for the nuclear case [4].

In Fig. (5) one shows the Glauber-Mueller dipole cross section as a function of the dipole size $r = \alpha r_\perp$ at two typical x_2 values. In the lower plot, for $x_2 = 10^{-2}$, the GM cross section underestimates the GBW one. However, as x_2 decreases the gluon distribution in the proton rises turning out the dipole cross section bigger. This feature is depicted in the upper plot, for a small $x_2 = 10^{-6}$, where GM overestimates GBW by a factor two at intermediate $r \sim 0.3$. An immediate consequence from the plots is that our predictions lies lower than GBW at $x_2 \approx 10^{-2}$ and higher for smaller x_2 . We discuss these features in a theoretical and phenomenological point of view when one performs the comparison with available data in the next section.

4. Results and Discussions

This section is devoted to perform theoretical predictions for the available data on

DY process and the forthcoming ones from RHIC or LHC. In the previous section, we presented a parameter-free Glauber-Mueller dipole cross section with matches leading log gluon evolution and contains corrections from unitarity effects (parton saturation) at higher energies. Therefore, we have a very clear dynamical understanding about the description of the observables depending on the gluonic content of the target, even if it is a nuclear one.

Although perturbative QCD provides reliable results at small distances (small dipole sizes), the nonperturbative sector is still far from being completely understood. The usual pdf's are evolved from a perturbative initial scale $Q_0^2 = M_0^2 \approx 1$ GeV 2 , and there is little information about the behavior at $Q^2 \leq Q_0^2$, where the perturbative description is not even justifiable. In general one makes use of Regge phenomenology to estimate those contributions (see, for instance [18]), and extrapolating to lower virtuality regions (large dipole sizes) one needs an ansatz regarding the nonperturbative sector.

This is the main justification of the use the GRV94 parametrization [26] in our calculations: bearing in mind that $Q^2 = 4/r^2$, its evolution initial scale is $Q_0^2 = 0.4$ GeV 2 , allowing to scan dipole sizes up to $r_{\text{cut}} = \frac{2}{Q_0} \text{ GeV}^{-1}$ ($= 0.62$ fm). The cut off $r_{(\text{cut})}$ means the scale matching the perturbative and nonperturbative sector. For the most recent parametrizations, where $Q_0^2 \sim 1$ GeV 2 ($r_{\text{cut}} \approx 0.4$ fm) the amount of nonperturbative contribution in the calculations should increase. An additional advantage is that GRV94 does not include non-linear effects to the DGLAP evolution since the parametrization was obtained from rather large x values. This feature ensures that the parametrization does not include sensible unitarity corrections (perturbative shadowing) in the initial scale.

Now, we should introduce an ansatz for the large transverse separation region. A more phenomenological way is to match the pQCD dipole cross section with the typical hadronic one $\sigma_{\pi N}$ at r_{cut} , for instance as performed in [18]. Nevertheless, due to the large growth of the pQCD dipole cross section at high energies and in order to be more consistent theoretically we choose an alternative way: the gluon distribution is frozen at scale r_{cut} , namely $x G(x, \tilde{Q}_{\text{cut}}^2)$. Then, the large distance contribution $r \leq r_{\text{cut}}$ reads as,

$$\sigma_{q\bar{q}}^{GM}(x, r \leq r_{\text{cut}}) = \frac{\pi^2 \alpha_s}{3} r_{\text{cut}}^2 x G_N^{GM}(x, \frac{4}{r_{\text{cut}}^2}). \quad (4.1)$$

In a more rigorous analyses, one should substitute the freezing scale \tilde{Q}_{cut}^2 for the saturation scale $Q_s^2(x)$ to take into account a realistic value of the gluon anomalous dimension in all kinematic region, still unknown.

To illustrate the role played by the small and large transverse separations in the description of the observables, in Fig. (6) one shows the profile of the r_{\perp} -integration from Eq. (2.11) as a function of the $\gamma^* q$ transverse separation r_{\perp} at typical mass M values. It is labeled here as $H_{T,L}(r_{\perp}, M^2)$. The momentum transfer is fixed at

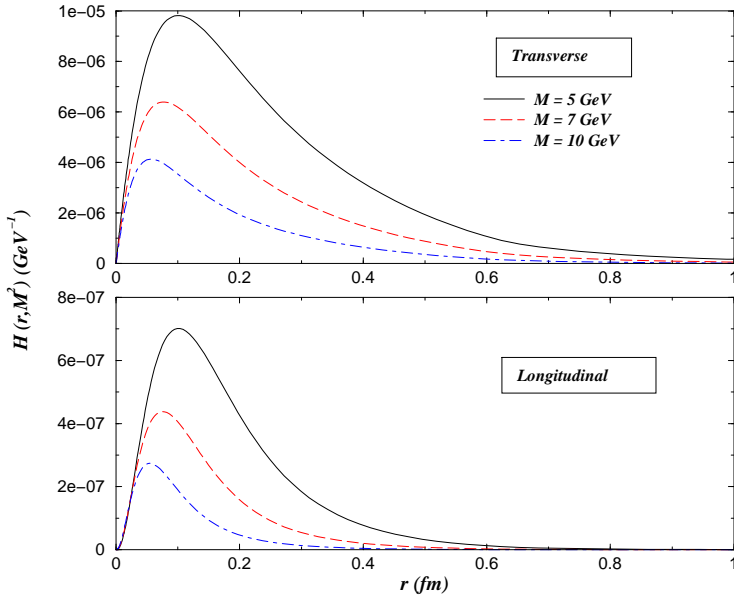


Figure 6: The profile $H_{T,L}(r_{\perp}, M^2)$ as a function of the γ^*q transverse separation r_{\perp} at typical mass M values. One uses $x_2 = 10^{-2}$ and GRV parametrization input. For discussions, see text.

$x_2 = 10^{-2}$, since the low x_2 data available lie at this magnitude. For the proton structure function $F_2^p(x_1/\alpha, M^2)$, describing the quark content of the projectile, we use the ALLM updated parametrization [28] (good agreement with HERA data at large x). Both transverse and longitudinal profiles are presented.

The main contribution for the profiles comes from the asymmetric peaks which are shifted to larger r_{\perp} as M diminishes. For instance, in the transverse profile, the peak lies at $r_{\perp} \approx 0.06$ fm for $M = 10$ GeV whereas at $M = 5$ GeV it takes values $r_{\perp} \approx 0.1$ fm. As it was verified in Sec. (2), the longitudinal sector selects smaller transverse sizes r_{\perp} than the transverse one. Indeed, from the upper plot, it is getting non-zero contributions up to large $r_{\perp} \approx 1$ fm. The higher twist character of the longitudinal piece is verified through the magnitude scale of $H_L(r_{\perp}, M^2)$. Due to the fact that the nonperturbative sector dominates for $r_{\text{cut}} = (\alpha r_{\perp})_{\text{cut}} \geq 0.62$ fm using the GRV input, a significant part of the contributions comes from the soft region where α is small (soft quark). This is in agreement with the expectations that important soft contributions take place in Drell-Yan process (see related discussions at [29]).

Now, we are able to compare the results with the available data. Since the color dipole picture is valid at small momentum fraction x_2 , one needs to select the experimental data covering this requirement. The lowest x_2 data measured were carried out by the fixed-target dimuon production at E772 Collaboration [17], where we select the points with $x_2 < 0.1$ following the similar procedure of [16]. In Fig. (7), one presents the calculation Eq. (2.11) using the Glauber-Mueller dipole cross

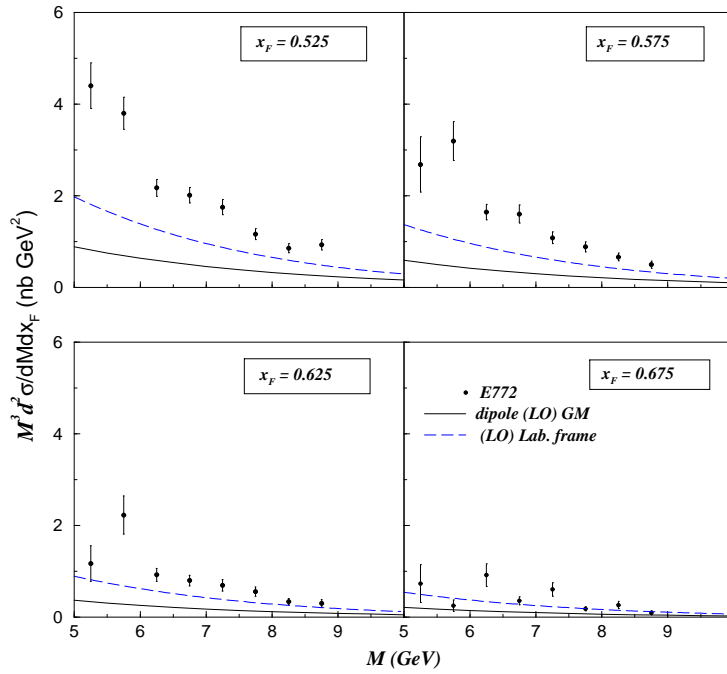


Figure 7: The DY differential cross section per nucleon versus M at the available small x_2 data [17] ($\sqrt{s} = 38.8$ GeV) at fixed x_F in pd reaction. The solid line corresponds to the Glauber-Mueller dipole cross section whereas the dashed one is the LO Breit system calculation.

section (the solid line) at fixed x_F and center of mass energy $\sqrt{s} = 38.8$ GeV ($0.03 \leq x_2 \leq 0.09$). It should be stressed that this kinematical region scans the validity limit of the color dipole picture.

The curves underestimate similar calculations in Ref. [16], which uses the phenomenological GBW dipole cross section. Such a result is actually expected from our conclusions in the previous section where GM underestimate GBW at $x_2 = 10^{-2}$ [see lower plot in Fig. (5)]. Indeed, we should introduce a K -factor in order to take into account higher orders corrections. We notice that using such a correction factor ($K \approx 2$) our results turn out similar to [16]. Moreover, it is claimed that GBW contains nonperturbative and higher order contributions built-in the parametrization, thus it does not require NLO correction factor [16].

Here, some comments about higher order corrections are timely. The color dipole approach results for total (virtual) photon cross section are equivalent to those ones obtained by k_T -factorization [20] in the leading logarithmic approximation. However, the inclusion of higher order effects in the k_T -factorization approach turns the equivalence incompatible: the conservation of the transverse positions and sizes of the colliding objects is violated [30]. Therefore, the introduction of higher orders contributions into the dipole cross section must be taken with some care. Moreover, deep inelastic and Drell-Yan have a quite different scenario concerning NLO and

NNLO corrections. In DIS, calculations considering up to NNLO resummations have been performed and it was found that they are small [31]. Instead, in Drell-Yan even the NLO calculations produce corrections up to a factor about two, diminishing as the energy increases [7, 13].

In the plots (Fig. 7) one shows also the LO Breit system calculation [Eq. (2.1)] (the dashed line). The color dipole result lies below LO fast proton frame one at $x_2 \approx 10^{-2}$ (where the presented data are available) because it considers only sea quarks from the target ($G \rightarrow q\bar{q}$ splitting). Thus, in this kinematical region the valence quark content competes with the the sea one and such a difference is expected. As x_2 decreases the gluonic content of the target drives the observables and the color dipole should produce quite reliable results. Such a kinematical window will be open by the new high energy acellerators RHIC and LHC allowing to probe the color dipole phenomenology properly.

In order to address the issue above, the DY differential cross section for RHIC energies, $\sqrt{s} = 500$ GeV, is shown in Fig. (8) for the same fixed x_F . There, the x_2 takes values of order 10^{-4} and unitarity effects are important. The solid lines are the Glauber-Mueller estimates and the dashed ones are the LO Breit calculations. No K factor is taken into account here. The curves overestimate similar calculations in Ref. [16], which uses the phenomenological GBW dipole cross section. Such a behavior is expected from our previous conclusions where GM overestimates GBW at smaller x_2 due to the growth of the gluon distribution at higher energies [see the upper plot in Fig. (5)]. Concerning the LO lab. calculations, the Glauber-Mueller underestimates them due to the significant corrections coming from unitarity effects (parton saturation). Although, we naively would expect that both are equivalent if no saturation effect is introduced in the gluon distribution. From the plots one verifies that the deviations are more significant as M diminishes, corresponding to smaller x_2 values. For instance, at $M = 5$ GeV the corrections reach a factor of about 15 % for $x_F = 0.525$ whereas at $x_F = 0.675$ they reach a factor around 30 %, meaning significant effect.

As final comments, we address additional advantages of the color dipole picture in the DY case. For example, it allows to obtain the transverse momenta p_T distribution for the process already at leading order calculation [16]. Instead, in the parton model the lepton pair has no transverse momentum due to the assumption that in the partonic subprocess the longitudinal momenta are bigger than the transverse ones (partons are collinear). There, an alternative way to solve this trouble is to introduce an intrinsic p_T for the initial state interacting partons. However, such an assumption is not sufficient to describe the measured p_T distributions. Considering the Compton and the annihilation subprocess the leptons acquire transverse momentum and the p_T -dependence can be calculated in pQCD. The resummations produce $\alpha_s \ln^2(m^2/p_T^2)$ terms which are large as the transverse momentum goes to soft values $p_T \rightarrow 0$ (the perturbative expansion breaks down). Thus, the color dipole

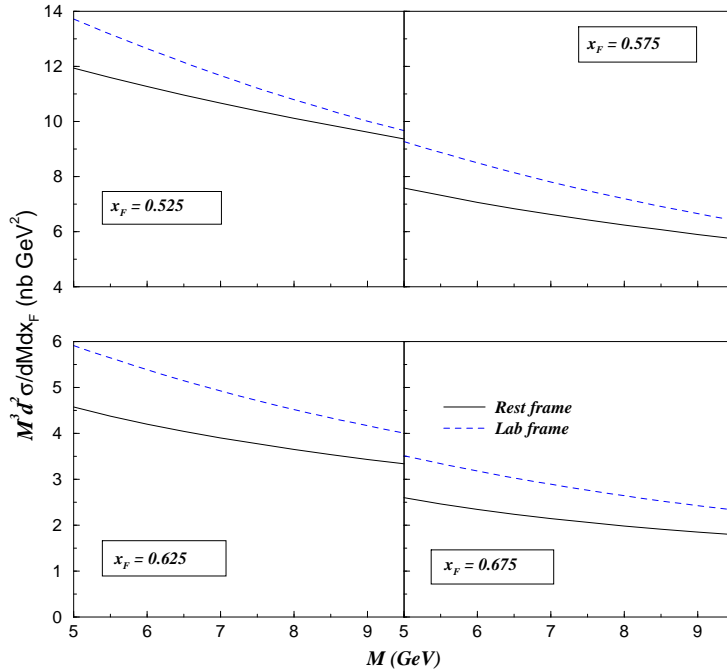


Figure 8: The DY differential cross section per nucleon versus M for the RHIC energies ($\sqrt{s} = 500$ GeV) at fixed x_F in pd reaction. The solid line corresponds to the Glauber-Mueller dipole cross section whereas the dashed one is the LO Breit system calculation.

description is a nice tool to calculate that distributions since the above difficulties are avoided.

5. Conclusions

The Drell-Yan is an important process testing the quark (antiquark) content of the hadron target. The measured observables are Lorentz invariant, whereas the parton description is frame dependent. Calculations in the fast proton system have provided a perturbative understanding of DY up to higher orders. On the other hand, the color dipole picture allows a simple description of DY driven by the gluonic content (sea quarks) of the target. The quark from the projectile radiates a photon decaying into a lepton pair. The basic blocks in the color dipole are the LC wavefunctions and the dipole cross section. The former is calculated from perturbation theory and the latter one is modeled taking into account general properties of both hard and soft domains.

We have found that the LC wavefunction for the γ^*q configuration plays the role of a weight for the different transverse separations r_\perp (as well as dipole sizes αr_\perp) contribution to the process. Namely, small transverse separations are selected by both the transverse and longitudinal pieces. However, the transverse one can select

non-negligible large sizes r_\perp . In addition, larger invariant mass M scans smaller γ^*q separations. Moreover, the longitudinal piece is higher twist (suppressed by a factor $1/M^2$). These features also present in the deep inelastic case due to the similarity between the LC wavefunctions expressions.

Concerning the dipole cross section, here we consider the Glauber-Mueller approach, which takes into account the corrections to the standard DGLAP formalism due to the unitarity requirements. The taming of the parton distributions (parton saturation) at high energies is performed considering the multiscattering assumption from the Glauber-like (eikonal) formalism. We have found a distinct behavior at both low and large x_2 when performing a comparison with the phenomenological GBW model. The main source of the deviation is that GM depends on the gluon distribution, which increases as x_2 diminishes. These features produce distinct results at current energies and in the forthcoming measurements. An important verification is that a non-negligible amount of non-perturbative contribution is present in the cross section. Although the LC wavefunctions suppress large transverse separations, a large cross section at small x_2 compensates the suppression producing significant soft content.

The current low x_2 available data lie in values ranging from $0.03 \leq x_2 \leq 0.09$, actually testing the validity limit of the color dipole picture. Our results underestimate the experimental measurements since color dipole includes only the sea quark content (gluon radiation) from the target. In the realistic case, for this kinematical region the valence and sea quarks have both a significant contribution in the cross section. It was found that issues related to higher orders contributions should be taken carefully.

As the energy reached in the forthcoming experiments increases, the saturation effects should turn out more evident. We perform estimates for the RHIC energies and have found that our predictions overestimate those ones using the GBW model, since in terms of the gluon distribution at higher energies (smaller x_2), when compared with the LO Breit system calculations one verifies corrections reaching about 30 % at low M (low x_2 and $x_F = 0.675$) region.

The quite simple scenario for DY process at rest frame allows to extend the approach to the nuclear case and also get information on p_T distribution. The higher energies to be available will demand a well established knowledge about the nuclear gluon distribution which can be the input for the nuclear dipole cross section in the color dipole framework. Thus, it is a usefull tool to perform pQCD estimates for the future experimental measurements.

Acknowledgements

M.A.B. and M.V.T.M. acknowledge useful discussions with Victor Gonçalves. M.V.T.M.

also acknowledges Martin McDermott (Liverpool University-UK) for useful enlightenments. This work was supported by CNPq, BRAZIL.

References

- [1] M. Klein, *Int. J. Mod. Phys. A***15**S1, 467 (2000).
A.M. Cooper-Sarkar, R.C.E. Devenish and A. De Roeck, *Int. J. Mod. Phys A***13**, 3385 (1998).
- [2] Yu.L. Dokshitzer. *Sov. Phys. JETP* **46**, 641 (1977);
G. Altarelli and G. Parisi. *Nucl. Phys.* **B126**, 298 (1977);
V.N. Gribov and L.N. Lipatov. *Sov. J. Nucl. Phys.* **28**, 822 (1978).
- [3] A.H. Mueller, *Nucl. Phys.* **335**, 115 (1990).
- [4] A.L. Ayala, M.B. Gay Ducati, E.M. Levin, *Nucl. Phys.* **B493**, 305 (1997); *Nucl. Phys.* **B511**, 355 (1998).
M.B. Gay Ducati, V.P. Gonçalves, *Nucl. Phys.* **B557**, 296 (1999); *Nucl. Phys.* (Proc. Suppl.) **79**, 302 (1999).
- [5] A.L. Ayala, M.B. Gay Ducati, E.M. Levin, *Eur. Phys. J C***8**, 115 (1999).
A.L. Ayala, M.B. Gay Ducati, V.P. Gonçalves, *Phys. Rev.* **D59**, 054010 (1999).
M.B. Gay Ducati, V.P. Gonçalves, *Phys. Rev.* **C60**, 058201 (1999); *Phys. Lett.* **B466**, 375 (1999); *Phys. Lett.* **B487**, 110 (2000).
- [6] A.H. Mueller, *Nucl. Phys.* **B558**, 285 (1999); A.H. Mueller, hep-ph/0111244.
L.V. Gribov, E. M. Levin, M.G. Ryskin, *Phys. Rep.* **100**, 1 (1983);
Y. U. Kovchegov, *Phys Rev.* **D60**, 034008 (1999).
I. Balitsky, *Nucl. Phys.* **B463**, 99 (1996).
L. Mc Lerran and R. Venugopalan, *Phys. Rev.* **D49**, 2233, 3352 (1994); **50**, 2225 (1994); **53**, 458 (1996);
E. Iancu, A. Leonidov and L. Mc Lerran, *Phys. Lett.* **B510**, 133 (2001); *Nucl. Phys. A* **692**, 583 (2001);
E. Ferreiro, E. Iancu, A. Leonidov and L. McLerran, [hep-ph/0109115].
J. Jalilian-Marian *et al.* *Phys. Rev.* **D59**, 034007 (1999);
N. Armesto and M. A. Braun, *Eur. Phys. J.* **C20**, 517 (2001).
- [7] P.L. McGaughey, J.M. Moss, J.C. Peng, *Ann. Rev. Nucl. Part. Sci.* **49**, 217 (1999).
- [8] J.P. Blaizot, *Theory of the Quark-Gluon Plasma*, [hep-ph/0107131].
- [9] N. Arnesto, A. Capella, E.G. Ferreiro, *Phys. Rev.* **C59**, 395 (1999).
- [10] N.N. Nikolaev, B.G. Zakharov, *Z. Phys.* **C49**, 607 (1991); *Phys. Lett.* **B260**, 414 (1991); *Z. Phys.* **C53**, 331 (1992).

[11] B.Z. Kopeliovich, In proceedings *Workshop Hirschegg'95: Dynamical Properties of Hadrons in Nuclear Matter..* Ed. by H. Feldmeier and W. Nörenberg, Darmstadt, p. 102 (1995).
 S.J. Brodsky, A. Hebecker, E. Quack, *Phys. Rev.* **D55**, 2584 (1997).
 B.Z. Kopeliovich, *Phys. Lett.* **B447**, 308 (1999).

[12] S.D. Drell, T.M. Yan, *Phys. Rev. Lett.* **25**, 316 (1970).

[13] A. Vogt, *Phys. Lett.* **B497**, 228 (2001).
 P.J. Rijken, W.L. van Neerven, *Phys. Rev.* **D51**, 44 (1995).

[14] G.R. Kerley, M. McDermott, *J. Phys.* **G26**, 683 (2000).
 M.F. McDermott, Los Alamos preprint [hep-ph/0008260].

[15] K. Golec-Biernat, M. Wüsthoff. *Phys. Rev.* **D59**, 014017 (1999); *Phys. Rev.* **D60**, 114023 (1999).

[16] B.Z. Kopeliovich, J. Raufeisen, A.V. Tarasov, *Phys. Lett.* **B503**, 91 (2001).

[17] E772 Collaboration, P.L. McGaughey et al., *Phys. Rev.* **D50**, 3038 (1994); erratum *Phys. Rev.* **D60**, 119903 (1999).

[18] M. McDermott et al., *Eur. Phys. J.* **C16**, 641 (2000).
 L. Frankfurt, M. McDermott, M. Strikman, *JHEP* **0103**, 045 (2001).

[19] E.A. Kuraev, L.N. Lipatov and V.S. Fadin. *Phys. Lett.* **B60** 50 (1975); *Sov. Phys. JETP* **44** 443 (1976); *Sov. Phys. JETP* **45** 199 (1977);
 Ya. Balitsky and L.N. Lipatov. *Sov. J. Nucl. Phys.* **28** 822 (1978).

[20] S. Catani, M. Ciafaloni, F. Hautmann, *Nucl. Phys.* **B366**, 135 (1991).
 J.C. Collins, R.K. Ellis, *Nucl. Phys.* **B360**, 3 (1991).

[21] A. Donnachie, P.V. Landshoff, *Phys. Lett.* **B437**, 408 (1998).

[22] M.B. Gay Ducati. *Braz. J. Phys.* **31**, 115 (2001) [hep-ph/0107116].

[23] A. Kovner, U. A. Wiedemann, *Phys. Rev.* **D64**, 114002 (2001).

[24] A.L. Ayala, M.B. Gay Ducati, E.M. Levin, *Phys. Lett.* **B388**, 188 (1996).
 M.B. Gay Ducati, V.P. Gonçalves, *Phys. Lett.* **B502**, 92 (2001).

[25] M.B. Gay Ducati, M.V.T. Machado, [hep-ph/0111093].

[26] M. Gluck, E. Reya, A. Vogt, *Z. Phys.* **C67**, 433 (1995).

[27] M.B. Gay Ducati, V.P. Gonçalves, *Phys. Lett.* **B487**, 110 (2000).

[28] H. Abramowicz, E. Levin, A. Levy, U Maor, *Phys. Lett.* **B269**, 465 (1991).
 H. Abramowicz, A. Levy, *The ALLM parameterization of $\sigma_{tot}(\gamma^* p)$ - an update*, [hep-ph/9712415].

- [29] B.Z. Kopeliovich, *Phys. Lett.* **B447**, 308 (1999).
- [30] A. Bialas, H. Navelet, R. Peschanski, *Nucl. Phys.* **B593**, 438 (2001); *Nucl. Phys.* **B603**, 218 (2001).
- [31] G. Altarelli, R.D. Ball, S. Forte, *Nucl. Phys.* **B599**, 383 (2001).